Supporting Information

High Ionic Conductivity Conjugated Artificial Solid Electrolyte Interphase Enabling Stable Lithium Metal Batteries

Dong Yan[a], Yuhao Ma[a], Hao Wang[a], Weishang Jia[b], Xiaobin Niu[a], Haibo Wang[c, *], Wei Zou[d, *], Liping Wang[a, *]

[a] School of Materials and Energy, University of Electronic Science and Technology of China, Chengdu 610054, P. R. China.

[b] Key Laboratory of General Chemistry of the National Ethnic Affairs Commission, School of Chemistry and Environment, Southwest Minzu University, Chengdu, 610041, China.

[c] College of Energy, Soochow University, Suzhou 215006, P. R. China.

[d] Lithium Resources and Lithium Materials Key Laboratory of Sichuan Province, Chengdu 610065, China.

* Corresponding author.

Corresponding author at:

E-mail: wanghb@suda.edu.cn (H. Wang);

E-mail: zouwei@tianqi-welion.com (W. Zou);

E-mail: lipingwang@uestc.edu.cn (L. Wang).

Experiment

1. Materials

Battery-grade Lithium bis(trifluoromethanesulfonyl)imide (LiTFSI), Lithium Tetrafluoroborate ($LiBF_4$), Lithium difluoro(oxalato)borate (LiDFOB), Ethylene glycol dimethyl ether (DME), 1,3-Dioxolane (DOL), Diethylcarbonate (DEC), and Fluoroethylene carbonate (FEC) were received from Suzhou DoDoChem Technology Co., Lt. Polyacrylonitrile (PAN) was purchased from Macklin (Mw=8w, AR). N, N-Dimethylformamide (DMF, AR) and $Zn(Ac)_2$ (AR) were purchased from Aladdin.

2. Synthesis of CPAN@ZnO

2.1 Preparation of electrospinning solution:

First, 1 g PAN was dissolved into 10 mL DMF. Then, a certain amount of $Zn(Ac)_2$ was added into the above solution and stirred for 24h to form a uniform solution.

2.2 Electrospinning process:

The prepared spinning solution was poured into a 10 mL plastic syringe equipped with a 20 G (gauge) stainless steel needle. The needle was connected to a high voltage (30 kV) DC-power supply to initiate the electrospinning under the feeding rate of 0.025 mm min^{-1}. The distance between the needle and the tin was 15 cm.

2.3 Annealing process:

The obtained composite film was pre-oxidized in air at 260 °C for 1h, with a heating rate of 2°C min^{-1}.

3. Synthesis of CPAN

The CPAN was prepared using the same method without the adding of $Zn(Ac)_2$.

4. Materials Characterization

The crystallographic phases of the samples were investigated by XRD (Bruker, D8 Advancer; Cu Kα, λ=1.54 Å). The micro-morphologies were characterized by SEM (SEM, USA-FEI Quanta FEG 250) and TEM (JEM2010F). The chemical states were investigated by XPS (Thermo Fisher Scientific Escalab 250Xi) and FT-IR (Thermo Scientific Nicolet iS50). The mass changes during annealing process and the interactions between PAN and $Zn(Ac)_2$ were obtained by STA (NETZSCH STA 449F5, the testing conditions for STA were identical to the annealing conditions for preparing CPAN@ZnO： 260 °C for 1h with a heating rate of 2°C/min).

5. Electrochemical Measurement

The electrochemical properties of the samples were tested using CR2032 coin-type cells with the separator of Celgard 2325 (thickness=25 μm, diameter=19 mm). The diameter of the Cu and NCM811 electrode is 11 mm. The amount of electrolyte was 50 uL and the voltage window of the full cell was 2.8-4.3V.

5.1 For Li||Cu asymmetrical cells:

The CPAN@ZnO layer was rolled on Cu foil, and 1M LiTFSI in DME/DOL 1:1 (v) with 2wt% $LiNO_3$ was used as the electrolyte.

5.2 For symmetrical cells:

The CPAN@ZnO layer was rolled on Li foils, and 1M LiTFSI in DME/DOL 1:1 (v) with 2wt% $LiNO_3$ was used as the electrolyte.

5.3 For anode-free full cells:

Full cells were assembled with NCM811 as cathode and Cu@CPAN@ZnO or Cu@CPAN or bare Cu as the anode. 0.6M $LiBF_4$ and 0.6M LiDFOB in FEC/DEC 1:2 (v) was used as the electrolyte.

For the cathode preparation, NCM811, acetylene black and polyvinylidene difluoride (PVDF) were mixed in N-methyl-2-pyrrolidone (NMP) at a weight ratio of 80:10:10, and the resulting slurry was cast on an aluminum foil followed by drying in a vacuum oven for 12h.

For the anode preparation, Li||Cu cells were first assembled, and 1 mAh/cm² of lithium was deposited onto the Cu@CPAN@ZnO\Cu@CPAN\bare Cu anode. The cell was then disassembled to retrieve the pre-lithiation anode, which was subsequently paired with an NCM811 cathode to assemble a full cell for anode-free battery testing.

5.4 Measurement

The galvanostatic charging/discharging of the cells was investigated on a Neware battery tester (CT-3008W). EIS measurements were performed by CHI660E with a frequency range of 0.01-10^5 Hz and an AC signal of 5 mV. The Tafel test was conducted by CHI660E using symmetric cells, with a voltage range of -0.3 to 0.3 V and a scan rate of 1 mV/s. And the Tafel formular as follows:

$$\eta = a + \mathrm{b}log(i)$$

where η is the overpotential, i is the current density, and b is the Tafel slope.

5.5 The electronic conductivity of CPAN@ZnO:

The electronic conductivity is measured using an symmetric cell configuration.[1] The current is below the minimum range of the test equipment (CHI660E), so the artificial SEIs are electronically insulated.

5.6 The ionic conductivity of CPAN@ZnO:

The ionic conductivity of SEl is based on EIS measurement of symmetrical cells. Ionic conductivity of the SEI layer can be calculated by using an equation:[2]

$$\sigma_{SEI} = \frac{2d_{SEI}}{R_{SEI}S_{SEI}} \tag{1}$$

where d is the thickness, R is the resistance, and S is the area of the SEl layer.

5.7 The Li$^+$ transfer number (t_{Li+}):

The t_{Li+} is characterized by the steady state polarization method in Li/Li cell with a polarization voltage of 0.01 V. according to the equation:[3]

$$t_{Li^+} = \frac{I_s(\Delta V - I_0R^0)}{I_0(\Delta V - I_sR^s)} \tag{2}$$

where I_0 and I_s are initial and steady-state current, which were recorded by chronoamperometry for 1000s. R^0 and R^s are interfacial resistance between the electrode and electrolyte before and after the test.

6. Theoretical Calculation

Density functional theory (DFT) calculations were performed using the Gaussian (G16) program with Becke's three-parameter hybrid method and the Lee-Yang-Parr correlation functional (B3LYP) at the 6-311++G(d,p) level. These calculations optimized the structures, determined the electrostatic potential (ESP), and calculated the binding energies.

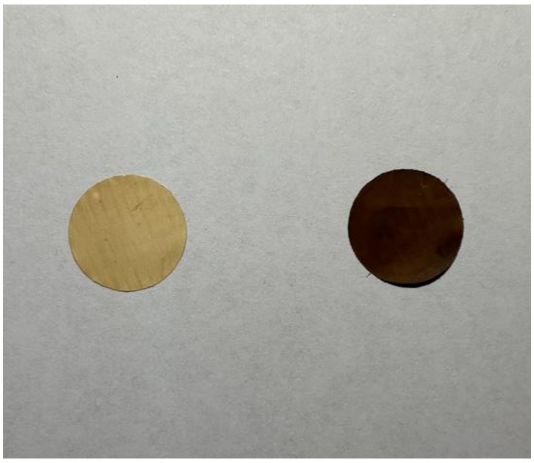

Fig. S1. Optical images of CPAN (left) and CPAN@ZnO (right).

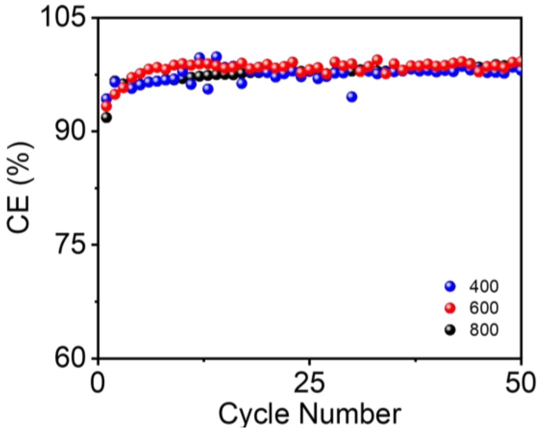

Fig. S2. CE test of different $Zn(Ac)_2$ additives.

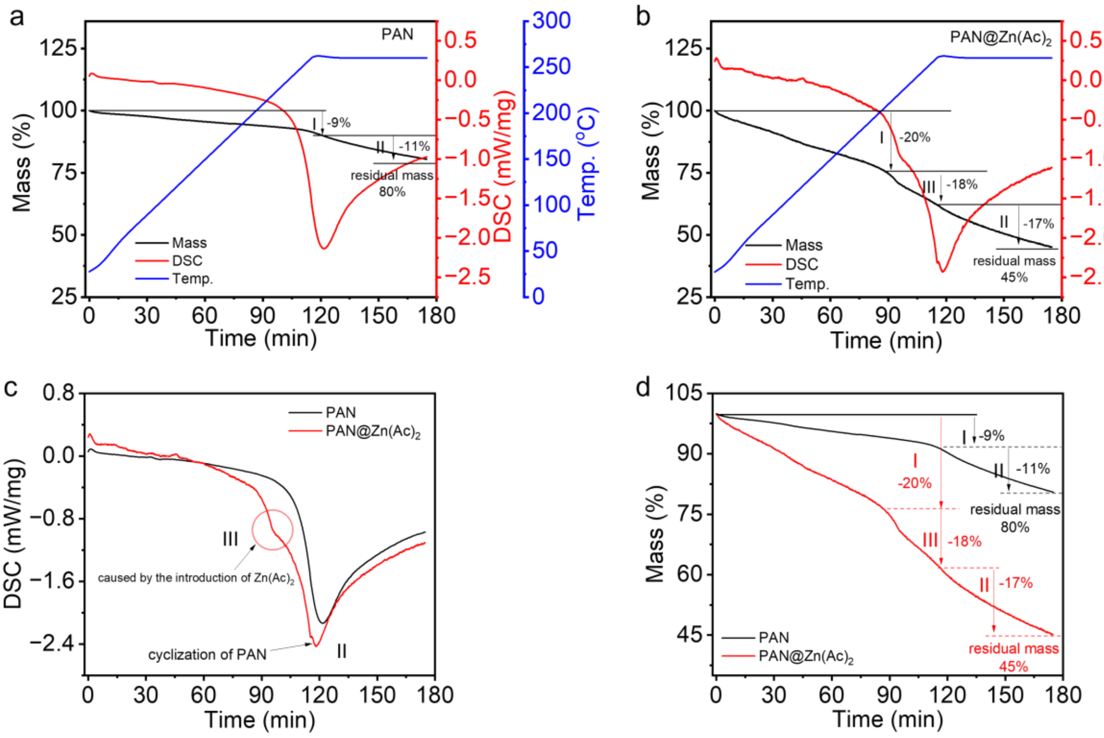

Fig. S3. Simultaneous Thermal Analysis. (a) PAN. (b) PAN@Zn(Ac)$_2$. Corresponding comparison of DSC (c), and TGA (d).

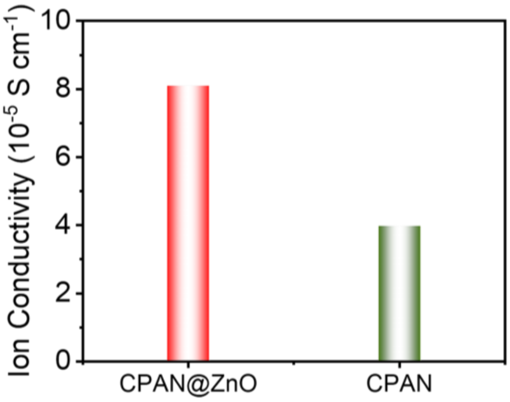

Fig. S4. Ionic conductivity of CPAN@ZnO and CPAN.

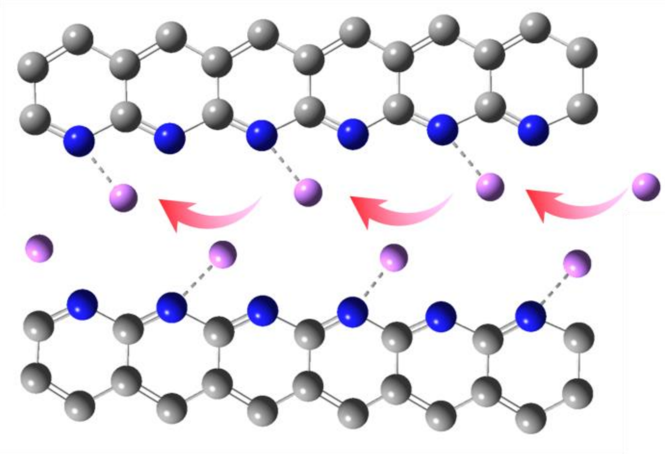

Fig. S5. The transport mechanism of Li^+ in the CPAN conjugated structure.

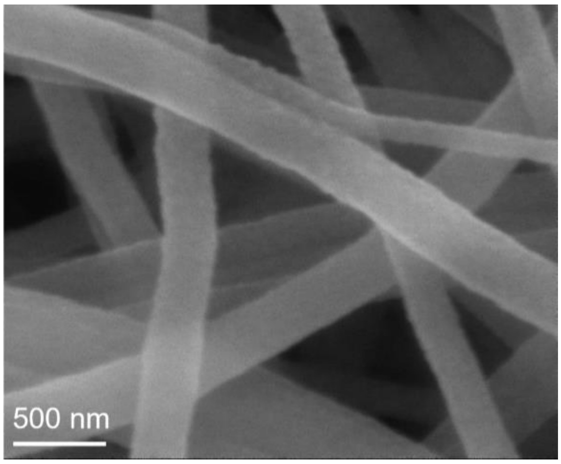

Fig. S6. SEM images of CPAN.

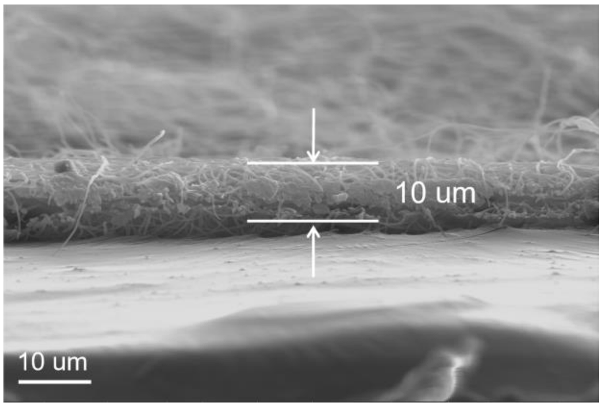

Fig. S7. Cross-view of CPAN@ZnO.

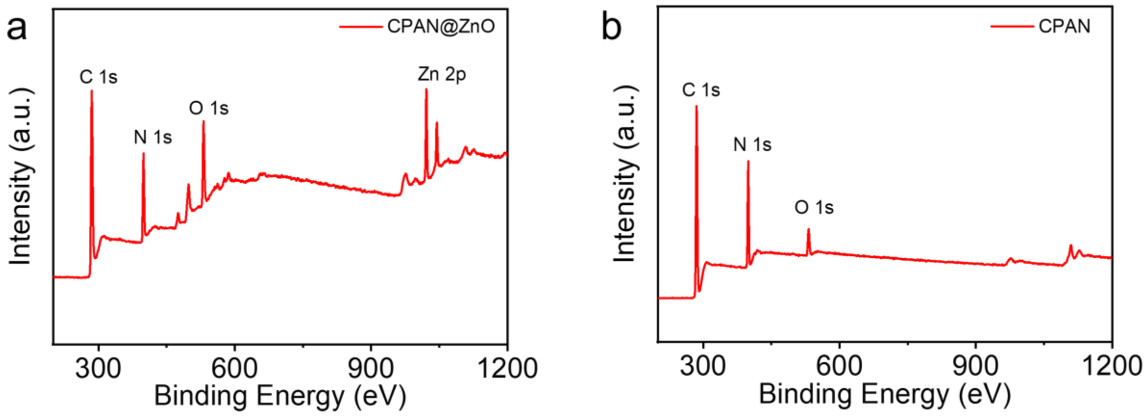

Fig. S8. XPS survey spectra before cycling. (a) CPAN@ZnO. (b) CPAN.

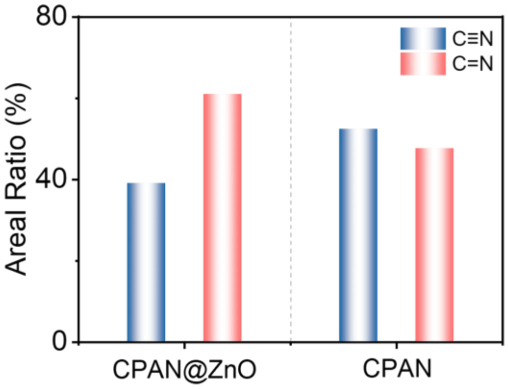

Fig. S9. The corresponding histograms of high-resolution for N 1s.

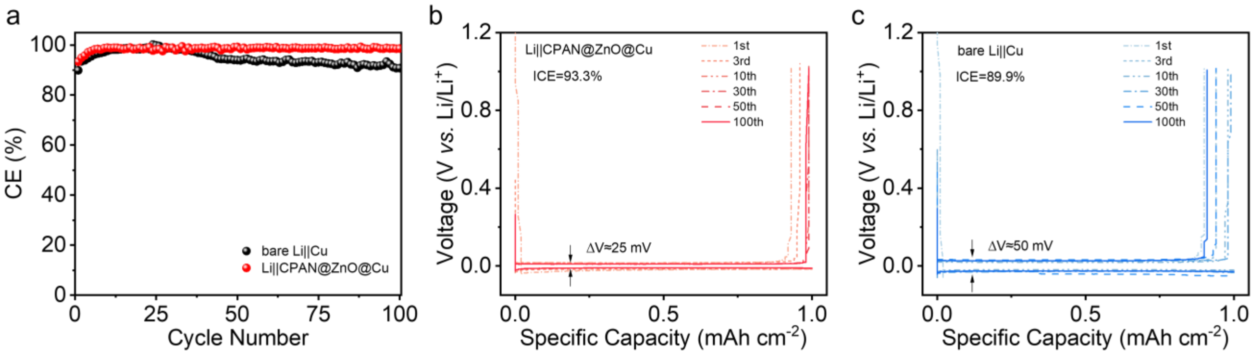

Fig. S10. CE test of Li||Cu batteries under 0.5 mA cm^{-2} and 1 mAh cm^{-2}. Charge/discharge curves at different cycling number of Li||CPAN@ZnO@Cu (b) and bare Li||Cu (c).

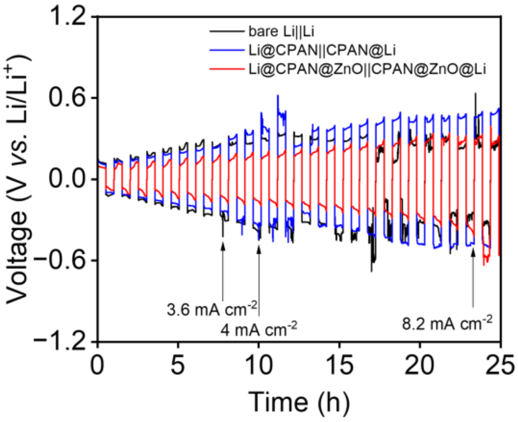

Fig. S11. Critical current density of symmetric cells.

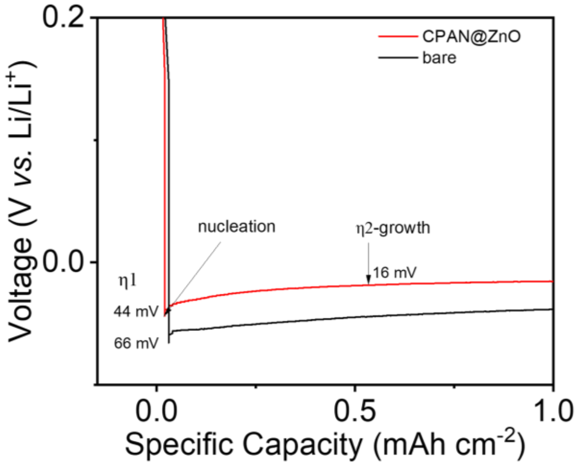

Fig. S12. Voltage profiles of the Li||Cu asymmetric cells at 0.5 mA cm^{-2}. Red line: Li||CPAN@ZnO@Cu, and black line: bare Li||Cu.

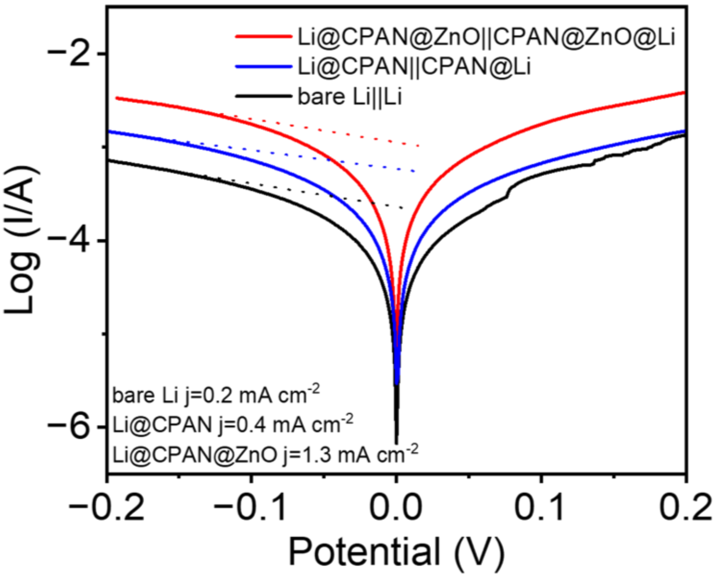

Fig. S13. Tafel curves of the Li symmetric batteries, and corresponding exchange current density.

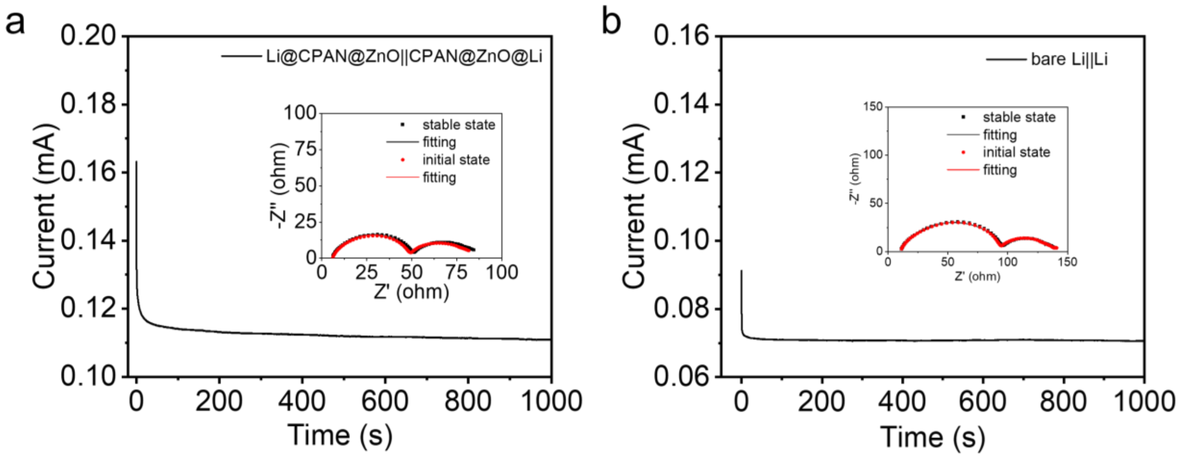

Fig. S14. The current evolution of Li symmetric cells under a polarization voltage of 10 mV and the related Nyquist plots before and after testing. (a) Li@CPAN@ZnO||CPAN@ZnO@Li. (b) bare Li||Li.

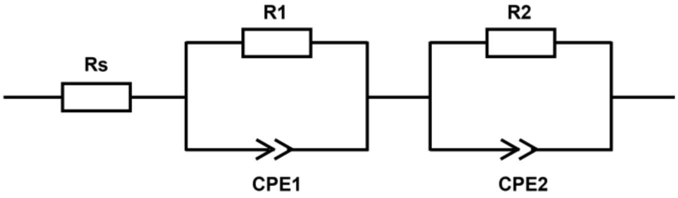

Fig. S15. The equivalent circuit diagram of symmetric cells.

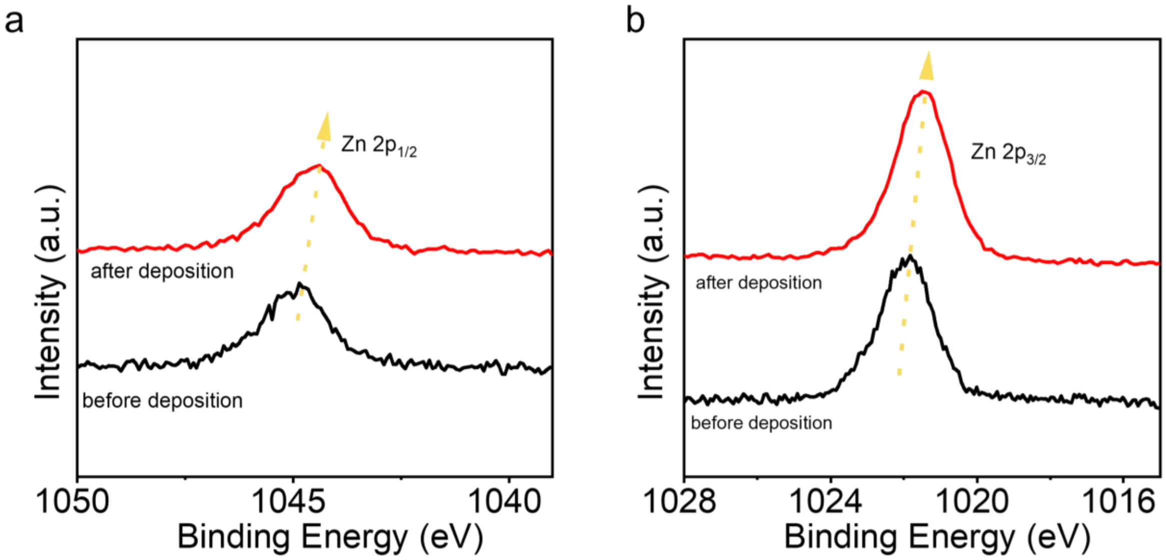

Fig. S16. High-resolution XPS spectra of Zn 2p for CPAN@ZnO.

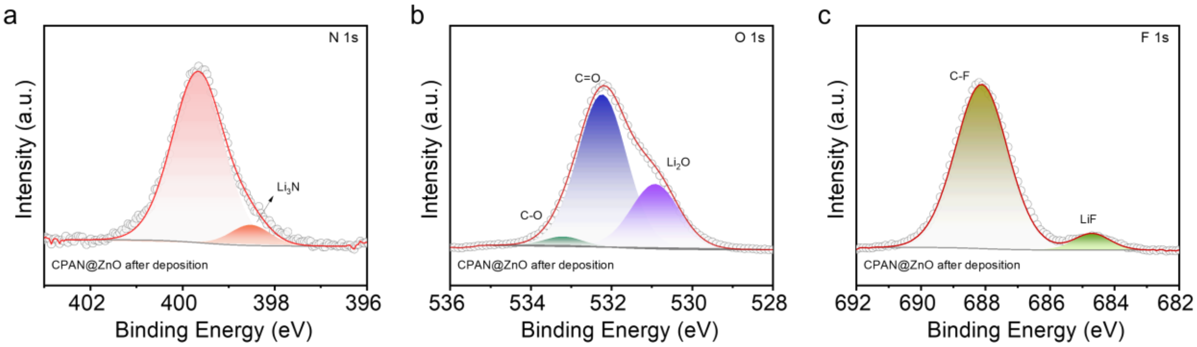

Fig. S17. High-resolution XPS spectra of CPAN@ZnO after Li deposition. (a) N 1s. (b) O 1s. (c) F 1s.

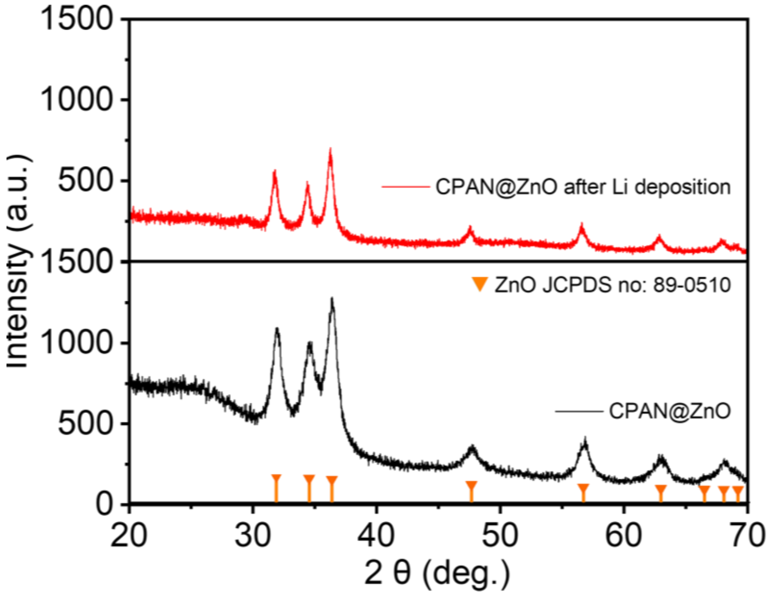

Fig. S18. XRD patterns of CPAN@ZnO before and after Li deposition.

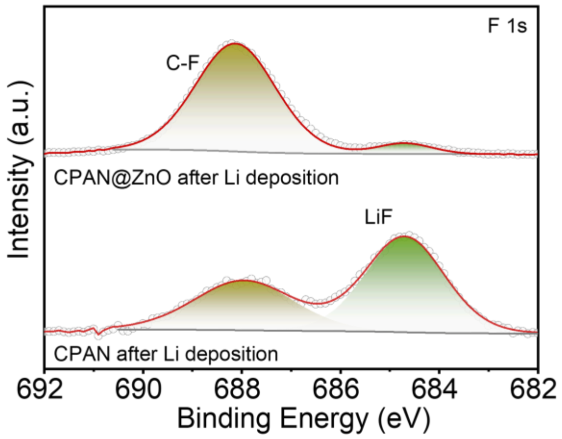

Fig. S19. High-resolution XPS spectra for F 1s.

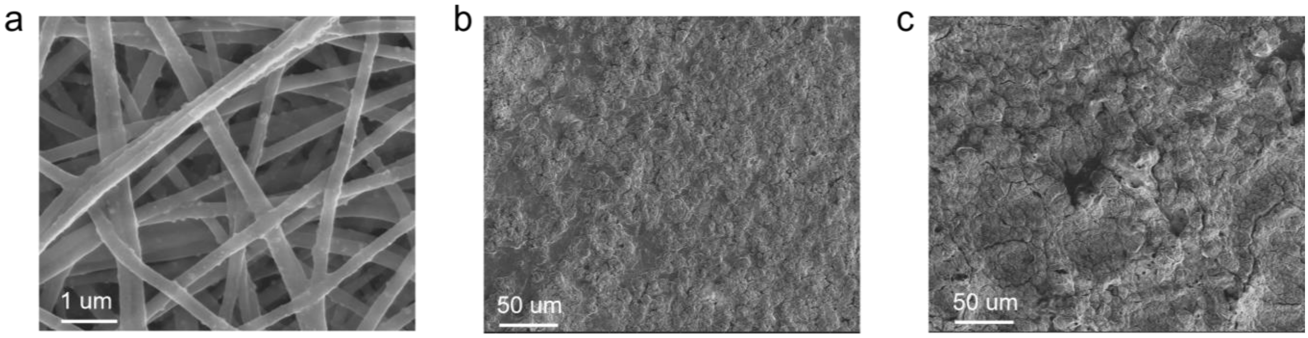

Fig. S20. The surface micromorphology after cycling. (a) CPAN@ZnO. (b) Li metal surface with the protection of CPAN@ZnO artificial SEI. (c) Bare Li metal surface without the protection of CPAN@ZnO artificial SEI.

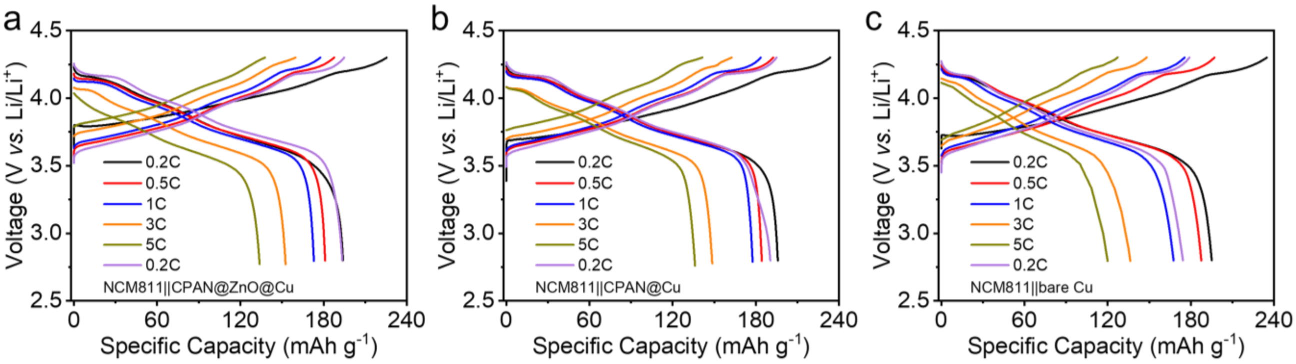

Fig. S21. The charging/discharging curves at different rates. (a) NCM811||CPAN@ZnO@Cu. (b) NCM811||CPAN@Cu. (c) NCM811|| bare Cu.

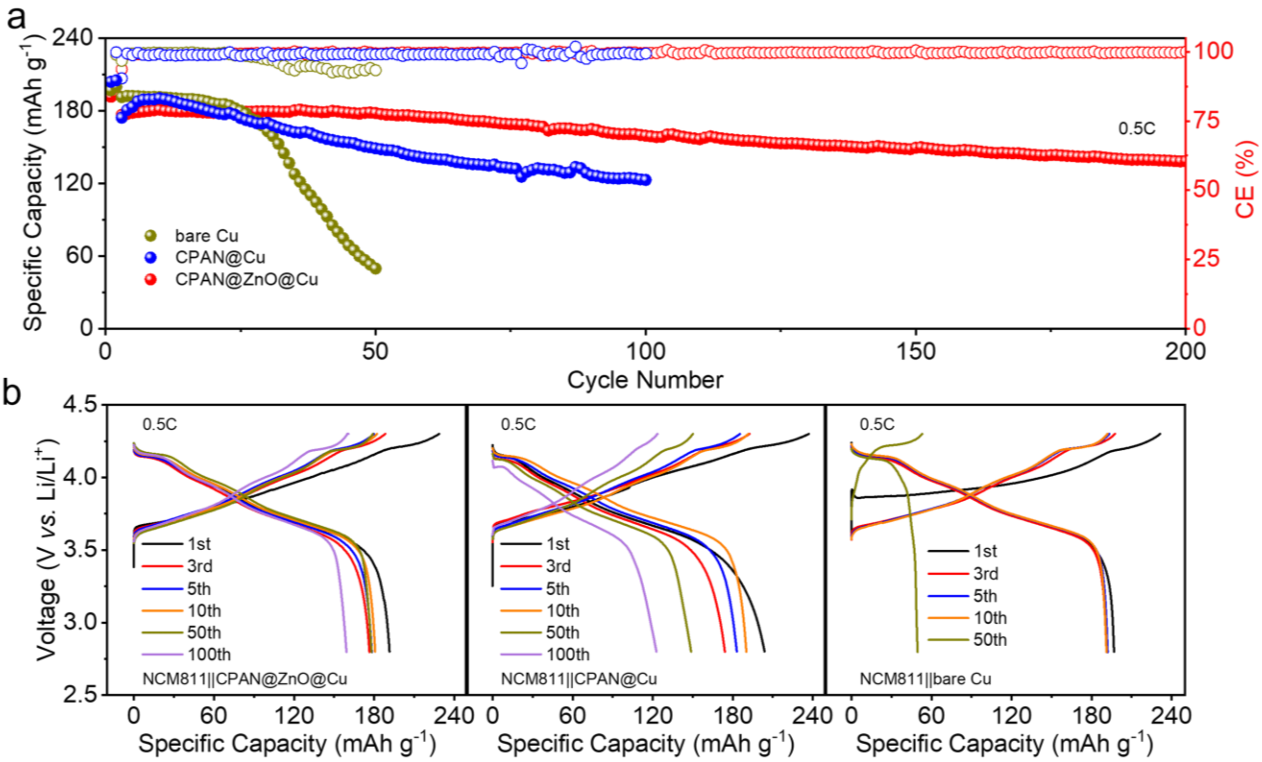

Fig. S22. The long cycling performance of full cells and corresponding charging/discharging curves.

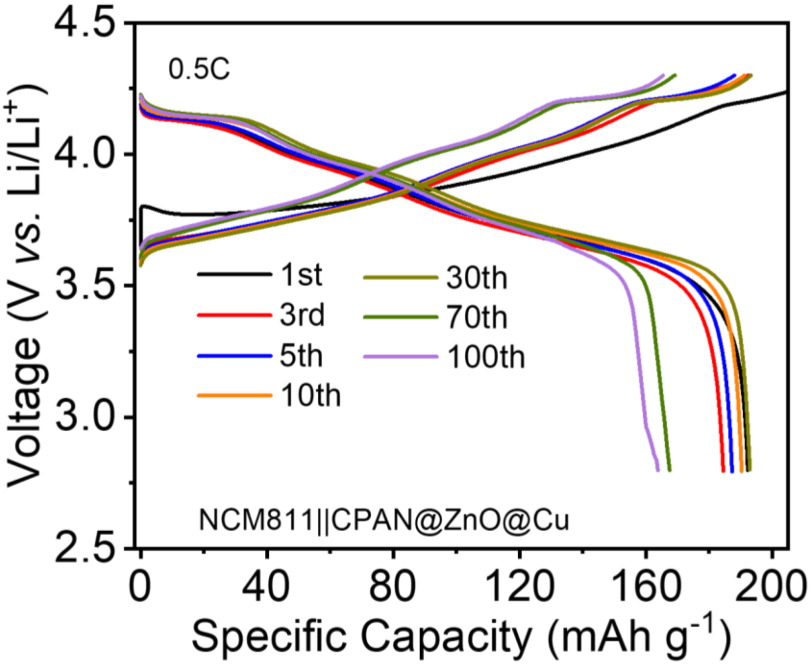

Fig. S23. The charging/discharging curves at 0.5C with an ultra-low N:P ratio of 0.6.

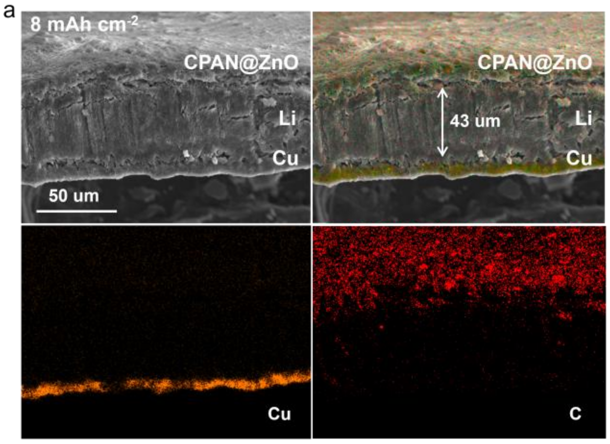

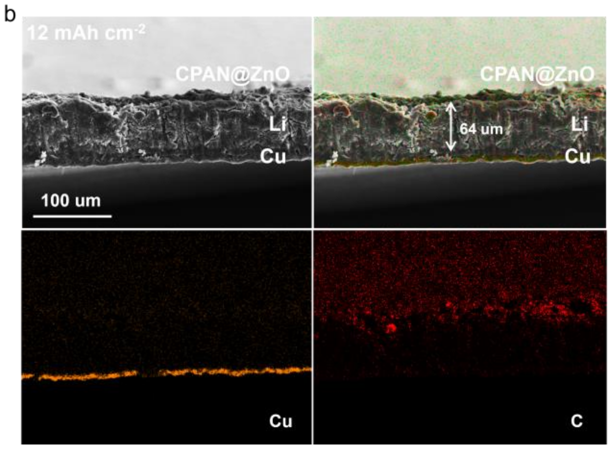

Fig. S24. The EDS of CPAN@ZnO@Cu after Li deposition. (a) After deposition of 8 mAh cm^{-2}. (a) After deposition of 12 mAh cm^{-2}.

Table S1. Comparison with conventional PAN-cyclization methods.

Temp. (°C)	Time (h)	Atmosphere	Ref.
260	**1**	**Air**	**our work**
350	2	Air	[4]
500	5	Ar	[5]
300	5	Ar	[6]
300	12	Ar	[7]
450	NA	N_2	[8]
280	2	Air	[9]
286	10	Ar	[10]
300	2	Air	[11]
350	3	N_2	[12]
300	10	Ar	[13]
450	NA	Ar	[14]

Table S2. EIS fitting results.

	state	**R1**	**R2**	**CPE1**	**CPE2**
Li@CPAN@ZnO||CPAN@ZnO@Li	initial state	42.74	32.18	0.81	0.76
	stable state	45.72	32.34	0.79	0.79
bare Li||Li	initial state	88.26	35.21	0.76	0.88
	stable state	85.96	42.06	0.77	0.77

Table S3. Cycling performance of symmetric cells with different SEIs reported before.

Materials	**Current density (mA cm^{-2})**	**Specific Capacity (mAh cm^{-2})**	**Overpotential (V)**	**Cycling life (h)**	**Reference**
CPAN@ZnO	**0.5**	**1**	**0.02**	**5400**	**This work**
	1	**4**	**0.025**	**3000**	
SN-SPE	0.2	1	0.05	1800	[15]
HFP	1	0.5	0.1	1400	[16]
NGCS	0.5	0.5	0.02	320	[17]
Li_3Bi-LiF	1	1	0.02	1000	[18]
PAN-b-PSBMA	0.5	0.5	0.1	700	[19]
$LiCu_x$	1	1	0.02	1200	[20]
ERS	1	1	0.1	2000	[21]
TPMS	1	1	0.03	1000	[22]
ZrOP	1	2	0.1	1600	[23]
DFNCA	0.5	0.5	0.05	1000	[24]
P(St-Mal)	1	1	0.15	1000	[25]
NMSF	1	1	0.025	1900	[26]
TEMED	0.5	1	0.05	3500	[27]
ZnF	1	1	0.05	500	[28]

Table S4. Comparison of cycling stability of full cells with different N/P.

Cathode	Anode	N/P	Voltage window (V)	Rate (C)	Cycle number	Capacity retention (%)	Ref.
NCM811	**Cu@CPAN@ZNO**	**0.6**	**2.8-4.3**	**0.5**	**100**	**89**	**Our work**
NCM811	Li	Sufficient Li	2.8-4.5	0.5	150	76	[29]
NCM811	Li	Sufficient Li	3-4.4	0.3	200	80	[30]
NCM811	Li	2.6	3-4.5	0.5	100	89	[31]
NCM811	Gr	3	3-4.3	1	200	72	[32]
NCM811	SiO*x*/G	1.2	2.5-4.3	0.5	100	88	[33]
NCM811	PI-Ag-Li	1	2.8-4.3	0.5	170	90	[34]
NCM811@C	Li	Sufficient Li	2.8-4.35	0.1	100	88	[35]
LS-NCM523	Gr	1.07	2.8-4.3	0.5/1	100	94	[36]
SS-NCM523	Gr	1.07	2.8-4.3	0.5/1	100	78	[36]
LFP	PGr-PP	1.1	NA	0.2	200	77	[37]

Notes and references

1 Y. Luo, S. Pan, J. Tian, Y. Liang, H. Zhong, R. Ma, J. Gu, Y. Wu, H. Zhang, H. Lin, W. Huang, Y. Deng, Y. Su, Z. Gong, J. Huang, Z. Hu and Y. Yang, *Adv. Mater.*, 2024, **36**, 2413325.

2 W. Ren, X. Shang, Y. Lin, H. Ren, L. Zhang, H. Su, Q. Li, L. Zhi, M. Wu and Z. Li, *Adv. Energy Mater.*, 2024, DOI: 10.1002/aenm.202405284, 2405284.

3 M. Li, S. Li, D. Yan, Y. Ma, X. Niu and L. Wang, *Chemical Science*, 2025, **16**, 2609-2618.

4 Y. Kang, J. Chen, S. Feng, H. Zhou, F. Zhou, Z. Low, Z. Zhong and W. Xing, *J. Membr. Sci.*, 2022, **662**, 120985.

5 C. Hong, R. Tao, S. Tan, L. A. Pressley, C. A. Bridges, H. Li, X. Liu, H. Li, J. Li, H. Yuan, X. Sun and J. Liang, *Adv. Funct. Mater.*, 2024, **35**, 2412177.

6 J. Wang, Q. Yuan, Z. Ren, C. Sun, J. Zhang, R. Wang, M. Qian, Q. Shi, R. Shao, D. Mu, Y. Su, J. Xie, F. Wu and G. Tan, *Nano Lett.*, 2022, **22**, 5221-5229.

7 K. Zhang, W. Cao, J. Wang, Z. Zhao, W. Yin, Z. Lv, J. Zhang, R. Wang, F. Wu and G. Tan, *Rare Met.*, 2025, **44**, 3575-3581.

8 T. Zhou, S. Wang, Y. Ao, B. Lan, Y. Sun, G. Tian, T. Yang, L. Huang, L. Jin, L. Tang, W. Yang and W. Deng, *Nano Energy*, 2025, **138**, 110910.

9 Y. Kang, Z. X. Low, K. Zhou, S. Feng, D. Zou, Z. Zhong and W. Xing, *J. Membr. Sci.*, 2025, **725**, 123944.

10 J. Song, Z. Huang, T. Tian, X. Xiang, S. Zeng, S. Wang and H. Tang, *Nano Res.*, 2025, DOI: 10.26599/nr.2025.94907486.

11 J. Yang, S. Wang, L. Du, S. Bi, J. Zhu, L. Liu and Z. Niu, *Adv. Funct. Mater.*, 2024, **34**, 2314426.

12 X. Wang, Y. Qian, L. Wang, H. Yang, H. Li, Y. Zhao and T. Liu, *Adv. Funct. Mater.*, 2019, **29**, 1902929.

13 S. Ma, J. Zhao, Q. Gao, C. Song, H. Xiao, F. Li and G. Li, *Angew. Chem. Int. Ed.*, 2023, **62**, e202315564

14 K. Wang, T. Zhao, R. Lv, W. Tang, T. Yu, G. Chen, L. Li, F. Wu and R. Chen, *Adv. Energy*

Mater., 2024, **14**, 2401281.

15 R. Lin, Y. He, C. Wang, P. Zou, E. Hu, X.-Q. Yang, K. Xu and H. L. Xin, *Nature Nanotechnology*, 2022, **17**, 768-776.

16 Y. Xie, Y. Huang, Y. Zhang, T. Wu, S. Liu, M. Sun, B. Lee, Z. Lin, H. Chen, P. Dai, Z. Huang, J. Yang, C. Shi, D. Wu, L. Huang, Y. Hua, C. Wang and S. Sun, *Nat. Commun.*, 2023, **14**, 2883.

17 G. Hou, X. Ren, X. Ma, L. Zhang, W. Zhai, Q. Ai, X. Xu, L. Zhang, P. Si, J. Feng, F. Ding and L. Ci, *J. Power Sources*, 2018, **386**, 77-84.

18 Q. Ran, H. Zhao, J. Liu, L. Li, Q. Hu, J. Song, X. Liu and S. Kormarneni, *J. Energy Chem.*, 2023, **83**, 612-621.

19 Y. Zhan, Z. Liu, Y. Geng, P. Shi, N. Yao, C. Jin, B. Li, G. Ye, X. Zhang and J. Huang, *Energy Storage Materials*, 2023, **60**, 102799.

20 J. Xing, T. Chen, L. Yi, Z. Wang, Z. Song, X. Chen, C. Wei, A. Zhou, H. Li and J. Li, *Energy Storage Materials*, 2023, **63**, 103067.

21 K. Long, S. Huang, H. Wang, A. Wang, Y. Chen, Z. Liu, Y. Zhang, Z. Wu, W. Wang and L. Chen, *Energy Environ. Sci.*, 2024, **17**, 260-273.

22 C. Ma, S. Zou, Y. Wu, K. Yue, X. Cai, Y. Wang, J. Nai, T. Guo, X. Tao and Y. Liu, *Angew. Chem. Int. Ed.*, 2024, **63**, e202402910.

23 Y. Gu, J. Hu, M. Lei, W. Li and C. Li, *Adv. Energy Mater.*, 2023, **14**, 202302174.

24 W.-h. Hou, P. Zhou, H. Gu, Y. Ou, Y. Xia, X. Song, Y. Lu, S. Yan, Q. Cao, H. Liu, F. Liu and K. Liu, *ACS Nano*, 2023, **17**, 17527-17535.

25 T. Naren, G. C. Kuang, R. Jiang, P. Qing, H. Yang, J. Lin, Y. Chen, W. Wei, X. Ji and L. Chen, *Angew. Chem. Int. Ed.*, 2023, **62**, e202305287.

26 Q. Wang, M. Wu, Y. Xu, C. Li, Y. Rong, Y. Liao, M. Gao, X. Zhang, W. Chen and J. Lu, *Carbon Energy*, 2024, **6**, e576.

27 J. Pokharel, A. Cresce, B. Pant, M. Y. Yang, A. Gurung, W. He, A. Baniya, B. S. Lamsal, Z. Yang, S. Gent, X. Xian, Y. Cao, W. A. Goddard, K. Xu and Y. Zhou, *Nat. Commun.*, 2024, **15**, 3085.

28 C. Wei, Y. Xiao, Z. Wu, C. Liu, Q. Luo, Z. Jiang, L. Li, L. Ming, J. Yang, S. Cheng and C. Yu, *Science China Chemistry*, 2024, **67**, 1990-2001.

29 Y. Cui, Y. Wang, S. Gu, C. Qian, T. Chen, S. Chen, J. Zhao and S. Zhang, *J. Power Sources*,

2020, **453**, 227852.

30 H. Zeng, C. Chen, C. Xu, K. Tan, L. Yang, S. Zhang and M. Wu, *Nano Energy*, 2025, **141**, 111121.

31 S. Li, H. Hong, X. Yang, D. Li, Q. Xiong, D. Zhang, S. Wang, Z. Huang, H. Lv and C. Zhi, *Adv. Mater.*, 2025, DOI: 10.1002/adma.202504333, 202504333.

32 W. Zhang, T. Sun, T. Ma, W. Hao, Z. Zha, M. Cheng and Z. Tao, *Chem. Eng. J.*, 2024, **491**, 151946.

33 Q. Meng, M. Fan, X. Chang, H. Li, W. Wang, Y. Zhu, J. Wan, Y. Zhao, F. Wang, R. Wen, S. Xin and Y. Guo, *Adv. Energy Mater.*, 2023, **13**, 2300507.

34 Z. ChaoHui, G. YuJie, T. ShuangJie, W. YuHao, G. J. Chen, T. YiFan, Z. XuSheng, L. BoZheng, X. Sen, Z. Juan, W. LiJun and G. YuGuo, *Science Advances* 2024, **10**, eadl4842.

35 M. Yang, S. Zhao, P. Guo, M. Cui, H. Li, M. Wang, J. Wang, F. Wu and G. Tan, *Energy Storage Materials*, 2025, **78**, 104272.

36 M. Yoon, J. Park, W. Chen, Y. Huang, T. Dai, Y. Lee, J. Shin, S. Lee, Y. Kim, D. Lee, D. Shin, J. Cho, Y. Dong and J. Li, *Energy Environ. Sci.*, 2025, DOI: 10.1039/d5ee01086a.

37 S. Xu, Q. Fang, J. Wu, S. Weng, X. Li, Q. Liu, Q. Wang, X. Yu, L. Chen, Y. Li, Z. Wang and X. Wang, *Small*, 2023, **20**, 2305639.